
HYPERBOLIC STATISTICAL INFERENCE FOR TREATMENT EFFECTS WITH CIRCULAR BIOMARKER OF ASTIGMATISM

A PREPRINT

Buddhananda Banerjee*

Surojit Biswas [†]

Daitari Prusty[‡]

Department of Mathematics

Indian Institute of Technology Kharagpur, India-721302

Abstract

Circular biomarkers arise naturally in many biomedical applications, particularly in ophthalmology, where angular measurements such as astigmatism are routinely recorded. Similar directional variables also occur in the study of human body rotations, including movements of the hand, waist, neck, and lower limbs. Motivated by a clinical dataset comprising angular measurements of astigmatism induced by two cataract surgery procedures, we propose a novel two-sample testing framework for circular data grounded in hyperbolic geometry. Assuming von Mises distributions with either common or group-specific concentration parameters, we embed the corresponding parameter spaces into the Poincaré disk, an open unit disk endowed with the Poincaré metric. Under this construction, each von Mises distribution is mapped uniquely to a point in the Poincaré disk, yielding a continuous geometric representation that preserves the intrinsic structure of the parameter space. This embedding enables direct comparison of group distributions via hyperbolic distances, leading to natural and interpretable test statistics. We develop permutation-based tests for the common concentration case and bootstrap-based procedures for unequal concentrations. Extensive simulation studies demonstrate stable empirical size, strong consistency, and superior asymptotic power compared with existing competing methods. The proposed methodology is illustrated through a detailed analysis of the cataract surgery dataset, including a clinically informed restructuring of the original observations. The results highlight the practical advantages of incorporating hyperbolic geometry into the analysis of circular biomedical data and underscore the potential of geometry-aware inference for directional biomarkers.

Keywords Von Mises distribution, Hyperbolic geometry, Poincaré disk, Poincaré metric, Permutation test, Bootstrap test, Biomarker

*bbanerjee@maths.iitkgp.ac.in

[†]surojit23@iitkgp.ac.in/surojit23.iitkgp@gmail.com

[‡]25MA91F0225@kgpian.iitkgp.ac.in

1 Introduction

1.1 Clinical motivation and data description

A cataract is characterised by progressive opacification of the crystalline lens, resulting in partial or complete visual impairment. Cataract extraction with intraocular lens implantation is the standard treatment and is among the most frequently performed surgical procedures worldwide. Contemporary surgical techniques emphasise rapid visual rehabilitation and minimal operative trauma. Nevertheless, the removal of dense or sclerotic cataracts continues to present technical challenges, particularly in resource-limited settings. Small incision cataract surgery (SICS) is a widely adopted technique in which the opacified lens is removed through a self-sealing scleral incision. In manual SICS, the incision typically ranges from 5.5 mm to 7 mm. Following prolapse of the lens nucleus into the anterior chamber, extraction is commonly performed using the irrigating VERTICS technique, which combines controlled fluid dynamics with mechanical assistance [Srinivasan \(2009\)](#). Alternative approaches include the SNARE-based method introduced by [Keener \(1995\)](#), in which the nucleus is divided and removed using a loop fashioned from steel wire. Phacoemulsification (PE), introduced by [Kelman \(2018\)](#), employs ultrasonic energy to fragment the lens, allowing removal through a smaller incision and often resulting in faster visual recovery. Torsional PE further reduces surgical energy by using oscillatory rather than longitudinal motion. Despite these advantages, PE is less frequently employed in many developing regions owing to its higher cost, longer training requirements, and reduced effectiveness in eyes with advanced nuclear sclerosis. Consequently, SICS remains the preferred surgical modality in such contexts. Corneal incisions made during cataract surgery may alter corneal curvature, leading to surgically induced astigmatism. Astigmatism results in blurred or distorted vision due to unequal refractive power across different meridians of the cornea. Clinically, this may manifest as reduced visual clarity along specific orientations. In regular astigmatism, the two main meridians are perpendicular to each other, whereas in irregular astigmatism, they are not. Regular astigmatism is commonly classified into three types based on the orientation of the steepest corneal meridian. In *with-the-rule (WTR) astigmatism*, the vertical meridian is steeper than the horizontal, resembling an American football lying on its side; as a result, vertical lines are perceived more clearly than horizontal ones. In *against-the-rule (ATR) astigmatism*, the horizontal meridian is the steepest, analogous to an American football standing on its end, leading to clearer perception of horizontal lines. *Oblique astigmatism* occurs when the steepest meridian lies in an oblique orientation, typically between (120°) and (150°) or between (30°) and (60°). This form is often more visually disturbing because it distorts objects that are usually aligned along vertical or horizontal axes. This makes it more disorienting than either WTR or ATR astigmatism.

Optimal postoperative visual outcomes are generally associated with astigmatism axes near 0°, 90°, or 180°. To reflect these clinically meaningful orientations while accounting for the circular nature of angular data, we apply a fourfold angular transformation (mod 2π). This approach has been employed previously to evaluate surgical techniques, optimise allocation strategies, and predict the axis of astigmatism in cataract surgery studies (see [Biswas et al., 2016a, 2015](#); [Banerjee and Biswas, 2026](#)).

1.2 Existing method

[Biswas et al. \(2016a\)](#) and [Bakshi \(2010\)](#) present a carefully developed methodological framework for two-sample inference with circular responses, motivated by clinical trials in which angular outcomes arise naturally and treatment efficacy is determined relative to a clinically preferred direction. Their work addresses an important gap in the statistical literature, as much of the classical methodology for circular data focuses on direct comparison of mean directions rather than proximity to a target direction carrying substantive scientific meaning.

In this context, they provided a principled framework for two-sample inference with angular data by modelling treatment-specific responses as von Mises distributions,

$$\Theta_1 \sim \text{VM}(\mu_1, \kappa_1), \quad \Theta_2 \sim \text{VM}(\mu_2, \kappa_2),$$

without loss of generality, take the preferred direction to be $\mu_0 = 0$. Rather than comparing μ_1 and μ_2 directly, treatment comparison is formulated in terms of the expected circular distance from μ_0 , thereby aligning statistical inference more closely with clinical interpretability. Two distance measures are considered: the geodesic distance

$$d_1(\theta, 0) = \min\{|\theta|, 2\pi - |\theta|\},$$

and the cosine-based distance

$$d_2(\theta, 0) = 1 - \cos \theta.$$

While $E\{d_1(\Theta)\}$ does not admit a closed-form expression, the von Mises model yields a simple and tractable form for

$$E\{d_2(\Theta)\} = 1 - A(\kappa) \cos \mu, \quad A(\kappa) = \frac{I_1(\kappa)}{I_0(\kappa)},$$

which provides a natural basis for inference, where $I_r(\cdot)$ denotes the modified Bessel function of the first kind of order r .

Under the assumption of a common concentration parameter, $\kappa_1 = \kappa_2 = \kappa$, equality of expected distances from the preferred direction reduces to testing

$$H_0 : \cos \mu_1 = \cos \mu_2.$$

Exploiting classical asymptotic results for sample trigonometric moments, the authors use the joint asymptotic normality of sample sine and cosine means to derive a Z-type test statistic based on the difference of sample mean cosines. The resulting procedure is asymptotically normal with a consistently estimable variance, yielding a simple yet theoretically sound large-sample test for two-sample comparison of circular outcomes.

Recognising that the assumption of equal concentration parameters may be untenable in practice, Biswas et al. extend their methodology to the more challenging case where $\kappa_1 \neq \kappa_2$. In this setting,

$$E(\cos \Theta_1) - E(\cos \Theta_2) = A(\kappa_1) \cos \mu_1 - A(\kappa_2) \cos \mu_2,$$

so direct comparison of cosine means is no longer valid. To address this difficulty, the authors normalise the sample cosine means using consistent estimators of $A(\kappa)$ and apply a variance-stabilising transformation via the $\arccos(\cdot)$ function. This leads to a quadratic-form test statistic which, under suitable regularity conditions, is shown via the delta method to follow an asymptotic χ^2_1 distribution under the null hypothesis. This extension represents a notable methodological contribution, as formal procedures for treatment comparison relative to a preferred direction under unequal concentration had received little attention in the applied circular data literature.

To complement the parametric methods, the authors also consider a nonparametric benchmark based on the Mann-Whitney-Wilcoxon test applied to circular distances from the preferred direction. Although distribution-free procedures may entail some loss of efficiency when parametric assumptions are valid, their inclusion provides a useful robustness check and a valuable point of reference for applied researchers.

Overall, the methodological development of Biswas et al. (2016a) is rigorous and well motivated, combining clinically meaningful distance-based formulations with sound asymptotic theory. The proposed framework offers a principled and practically relevant approach to two-sample inference for circular responses, well aligned with the needs of applied medical statistics.

Notwithstanding these contributions, existing procedures remain largely dependent on parametric assumptions and asymptotic approximations, with inference driven primarily by trigonometric moments. In particular, there is a lack of stability with empirical labels when concentration parameters differ which is natural phenomena in real life scenario. For instance in the astigmatism data that they have analyzed has different concentration parameters in two competing groups, highlighting the need for alternative approaches that retain clinical interpretability while offering improved robustness.

1.3 Motivating Poincaré disk representation of von Mises parameters

We propose a novel and geometrically principled framework for two-sample inference with circular data, motivated by biomedical applications in which angular biomarkers play a central role. The methodology is distinguished by its elegant integration of directional statistics, hyperbolic geometry, and permutation-based inference, yielding a powerful and interpretable testing procedure with strong finite-sample properties.

Let $\Theta_{gi} \in [0, 2\pi)$ denote circular observations from group $g \in \{1, 2\}$, $i = 1, \dots, n_g$. We assume that within each group the data follow a von Mises distribution, $\Theta_{gi} \sim \text{VM}(\mu_g, \kappa_g)$, where μ_g is the mean direction and κ_g is the concentration parameter, allowing for either a common or group-specific concentration structure. Rather than comparing groups directly on the circle, the proposed method operates on the *parameter space* of the von Mises family, exploiting its natural geometric representation.

Specifically, for each pair (μ_g, κ_g) the von Mises distribution on the circle is parametrised by the mean direction $\mu_g \in [0, 2\pi)$ and the concentration parameter $\kappa_g \geq 0$. A natural and bijective mapping from these parameters to the Poincaré disk $\mathbb{D} = \{z \in \mathbb{C} : |z| < 1\}$ is given by via the transformation

$$\xi_g = \xi(\mu_g, \kappa_g) = r(\kappa_g) e^{i\mu_g}, \text{ where } r(\kappa_g) = \frac{\kappa_g}{1 + \kappa_g} \in [0, 1), g = 1, 2. \quad (1.1)$$

which embeds the circular model parameters into the Poincaré disk endowed with the hyperbolic metric

$$d_{\mathbb{H}}(w_1, w_2) = \cosh^{-1} \left(1 + \frac{2|w_1 - w_2|^2}{(1 - |w_1|^2)(1 - |w_2|^2)} \right), \text{ for all } w_1, w_2 \in \mathbb{D} \quad (1.2)$$

This representation provides a unified and non-Euclidean geometry in which both location and concentration differences are jointly captured, a key strength of the proposed approach. See Figure 1 for illustration.

When $\kappa = 0$, the von Mises distribution reduces to the uniform distribution on the circle. Under the mapping, $\xi = r(0)e^{i\mu} = (0, 0)$ independent of μ . This correctly reflects the fact that, when the concentration is zero, the mean direction is no longer meaningful; the distribution is uniform and location-invariant. Thus, the origin of the Poincaré disk corresponds uniquely to the uniform circular distribution. For small positive κ , the mapped points lie very close to the origin, with their direction encoding the mean angle μ , while the distance from the origin is an increasing function of the concentration. This ensures that the Poincaré disk faithfully captures both weakly concentrated distributions and their mean directions in a continuous manner as $\kappa_g \rightarrow 0^+$. As $\kappa \rightarrow \infty$, the von Mises distribution becomes increasingly concentrated around its mean μ_g , approaching a point mass. The mapping satisfies $\lim_{\kappa_g \rightarrow \infty} r(\kappa_g) = 1$, so the corresponding points approach the boundary of the Poincaré disk. The angular coordinate remains μ_g , encoding the mean direction, while the distance from the origin reflects the extreme concentration. Hence, the boundary of the disk naturally represents highly concentrated, nearly deterministic distributions. The origin $(0, 0)$ represents maximum uncertainty (uniform distribution). The proposed bijection (Equation 1.1) for each von Mises distribution corresponds

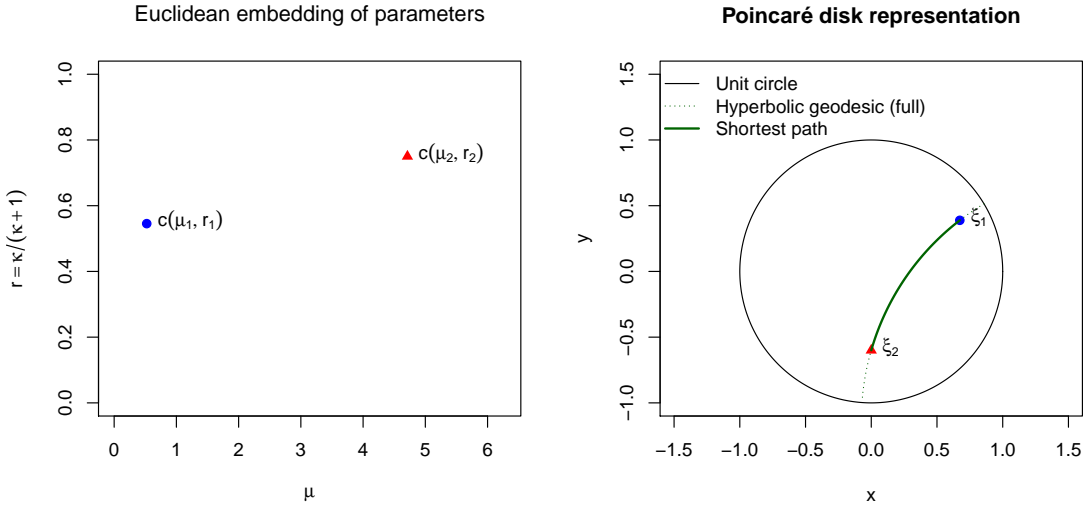


Figure 1: Mapping of the von Mises parameters to Poincaré disk

to a unique point in the Poincaré disk, and vice versa. Furthermore, the mapping is continuous in both parameters. Small changes in concentration or mean direction result in small changes in the disk, preserving the natural geometry of the parameter space.

Group differences are quantified through the hyperbolic distance between estimated parameter points, yielding a test statistic involving the plug-in estimator obtained from maximum likelihood estimates of (μ_g, κ_g) . To avoid reliance on asymptotic approximations and to ensure robustness in moderate sample sizes, inference is conducted using a permutation test that respects the circular structure of the data. Extensive simulations show that the proposed test attains accurate size over a broad range of settings and delivers improved power over existing circular two-sample procedures, particularly under unequal concentration or joint location–concentration alternatives. Importantly, the method remains stable for small to moderate sample sizes, underscoring its practical relevance for biomedical applications.

The methodology is further illustrated using astigmatism data from cataract surgery, where angular responses are clinically meaningful and inherently circular. By embedding the problem within a hyperbolic geometric framework, the proposed approach achieves both conceptual coherence and enhanced inferential performance, establishing a flexible and effective tool for analysing circular biomarkers in medical research.

1.4 Organization of the paper

Section 1.1 introduced the motivating astigmatism dataset arising from two cataract surgery procedures and outlines the statistical challenges inherent to circular biomarkers. Preceded by the existing work in Section 1.2, Section 1.3 develops the proposed geometric framework, detailing the hyperbolic embedding of von-Mises distributions into the Poincaré disk and establishing key properties of the mapping, including uniqueness, continuity, and interpretability. The rest of the paper is organized as follows.

Section 2 presents the proposed two-sample testing procedures, covering both equal and unequal concentration settings and describing the associated permutation and bootstrap implementations. Section 3 reports an extensive simulation study assessing empirical size stability and power across a wide range of sample sizes and concentration levels, with

systematic comparisons against existing methods. Section 4 applies the methodology to the cataract surgery data, including a clinically motivated restructuring of the dataset and a substantive interpretation of the results. Finally, Section 5 concludes with a discussion of the methodological contributions, practical implications, and potential extensions of hyperbolic geometric inference for circular biomedical data. The necessary technical proofs are available in Appendix (Section 6).

2 Methodology and Main result

As already introduced, let $\Theta_{gi} \in [0, 2\pi)$ denote circular observations from treatment group $g \in \{1, 2\}$, for $i = 1, \dots, n_g$. It is assumed that, within each group, the observations are independent and follow a von Mises distribution, $\Theta_{gi} \sim \text{VM}(\mu_g, \kappa_g)$, where μ_g denotes the mean direction and κ_g the concentration parameter of group g . The corresponding density function is given by

$$f(\theta | \mu_g, \kappa_g) = \frac{1}{2\pi I_0(\kappa_g)} \exp\{\kappa_g \cos(\theta - \mu_g)\}, \quad \theta \in [0, 2\pi), \quad (2.1)$$

where $I_0(\cdot)$ denotes the modified Bessel function of the first kind of order zero.

In many biomedical applications, the objective is not to compare mean directions directly, but rather to assess how closely each treatment aligns with a clinically desired and pre-specified direction, denoted by μ_0 . Within the Poincaré disk model \mathbb{D} of hyperbolic geometry, this preferred direction is represented by the radius $R_{\mu_0} = \{te^{i\mu_0} : 0 \leq t < 1\}$

Let $\xi_g \in \mathbb{D}$ denote the hyperbolic embedding corresponding to treatment group g . Treatment 1 is preferred over treatment 2 if the hyperbolic (Poincaré) distance between ξ_1 and the target radius R_{μ_0} is smaller than that between ξ_2 and R_{μ_0} , that is,

$$\min_{0 \leq t < 1} d_{\mathbb{H}}(\xi_1, te^{i\mu_0}) < \min_{0 \leq t < 1} d_{\mathbb{H}}(\xi_2, te^{i\mu_0}), \quad (2.2)$$

where $d_{\mathbb{H}}(\cdot, \cdot)$ denotes the Poincaré distance on \mathbb{D} as defined in the Equation 1.2. Moreover, we have,

Lemma 1 (Uniqueness of Minimizer). *For each $\xi \in \mathbb{D}$, the minimizer $\mathcal{P}_{\mu_0}(\xi) = \arg \min_{0 \leq t < 1} d_{\mathbb{H}}(\xi, te^{i\mu_0})$ is unique.*

Proof. See the Appendix 6.1. □

Denoting $d_{R_{\mu_0}}(\xi_g) = \min_{0 \leq t < 1} d_{\mathbb{H}}(\xi_g, te^{i\mu_0})$ for $g = 1, 2$; we state the null hypothesis $H_0 : d_{R_{\mu_0}}(\xi_1) = d_{R_{\mu_0}}(\xi_2)$ against the alternative $H_1 : d_{R_{\mu_0}}(\xi_1) \neq d_{R_{\mu_0}}(\xi_2)$. Since the true parameters (μ_g, κ_g) are unknown, they are estimated using the corresponding maximum likelihood estimators. Specifically, for $g = 1, 2$, the maximum likelihood estimators $(\hat{\mu}_g, \hat{\kappa}_g)$ are defined as

$$(\hat{\mu}_g, \hat{\kappa}_g) = \arg \max_{(\mu_g, \kappa_g)} \prod_{i=1}^{n_g} f(\theta_{gi} | \mu_g, \kappa_g), \quad (2.3)$$

where $f(\cdot | \mu_g, \kappa_g)$ denotes the von Mises density given in Equation (2.1).

Define the circular sample means

$$\bar{C}_g = \frac{1}{n_g} \sum_{j=1}^{n_g} \cos(\theta_{gj}), \quad \bar{S}_g = \frac{1}{n_g} \sum_{j=1}^{n_g} \sin(\theta_{gj}), \quad \bar{R}_g = \sqrt{\bar{C}_g^2 + \bar{S}_g^2}.$$

The maximum likelihood estimators admit the closed-form expressions

$$\hat{\mu}_g = \text{Arg} \left(\frac{1}{n_g} \sum_{j=1}^{n_g} e^{i\theta_{gj}} \right), \quad \hat{\kappa}_g = A_1^{-1}(\bar{R}_g),$$

where $A_1(\kappa) = I_1(\kappa)/I_0(\kappa)$. Further details may be found in [Mardia and Jupp \(2000\)](#).

In the specific context of the astigmatism data analysed in Section 1.1, the preferred direction is $\mu_0 = 0$, so that $R_0 = \{(t, 0) : 0 \leq t < 1\}$. Consequently, the minimum Poincaré distance reduces to

$$d_{R_0}(\hat{\xi}_g) = d_{\mathbb{H}}(\hat{\xi}_g, \mathcal{P}_{R_0}(\hat{\xi}_g)),$$

where $\mathcal{P}_{R_0}(\hat{\xi}_g)$ denotes the projection of $\hat{\xi}_g \in \mathbb{D}$ onto R_0 and can be obtained by the following lemma.

Lemma 2 (Projection along zero direction). *The projection any point $\xi \in \mathbb{D}$ on $R_0 = \{(t, 0) : 0 \leq t < 1\}$ is given by given by*

$$\mathcal{P}_{R_0}(\xi) = \left(\min \left\{ 1, \max \left\{ 0, \frac{1 + |\xi|^2 - \sqrt{(1 + |\xi|^2)^2 - 4 \Re(\xi)^2}}{2 \Re(\xi)} \right\} \right\}, 0 \right), \quad (2.4)$$

and $\Re(\xi)$ denotes the real part of ξ and $|\cdot|$ denotes the modulus of a complex number.

Proof. See the Appendix 6.2. □

These estimates are then used to construct the proposed test statistic

$$T = |d_{R_0}(\hat{\xi}_1) - d_{R_0}(\hat{\xi}_2)|, \quad (2.5)$$

where $\hat{\xi}_g$ is obtained by substituting the maximum likelihood estimators $(\hat{\mu}_g, \hat{\kappa}_g)$ into the embedding defined in Equation (1.1). The null hypothesis is rejected for the large value of the statistic. Notably, the statistic T remains well defined even when $\kappa_1 \neq \kappa_2$. Since a closed-form distribution of T is not available, statistical inference is carried out using a permutation-based procedure, which ensures accurate empirical size and improved power across a wide range of configurations. We summarize the theoretical consistency of the proposed test in the following theorem.

Theorem 1 (Consistency of the Poincaré Distance-Based Permutation Test). *Let $\{\Theta_{gi}\}_{i=1}^{n_g}$, $g = 1, 2$, be independent samples such that*

$$\Theta_{gi} \stackrel{iid}{\sim} VM(\mu_g, \kappa_g), \quad \kappa_g > 0,$$

and let $\xi_g \in \mathbb{D}$ denote the population-level embedding defined in equation (1.1). Consider the hypotheses

$$H_0: d_{R_0}(\xi_1) = d_{R_0}(\xi_2) \quad \text{versus} \quad H_1: d_{R_0}(\xi_1) \neq d_{R_0}(\xi_2),$$

and the test statistic

$$T = |d_{R_0}(\hat{\xi}_1) - d_{R_0}(\hat{\xi}_2)|,$$

where $\hat{\xi}_g$ is obtained by substituting the maximum likelihood estimators $(\hat{\mu}_g, \hat{\kappa}_g)$ for (μ_g, κ_g) .

Then the permutation test that rejects H_0 for large values of T is consistent in the sense that, for any fixed alternative satisfying $d_{R_0}(\xi_1) \neq d_{R_0}(\xi_2)$,

$$\lim_{\min\{n_1, n_2\} \rightarrow \infty} \mathbb{P}_{H_1}(\text{reject } H_0) = 1.$$

Proof. The proof proceeds by establishing convergence of the test statistic to a non-zero constant under H_1 and exploiting the invariance of the permutation distribution under H_0 . See the Appendix 6.3 for details. □

3 Simulation

The primary objective of the simulation study is to compare the proposed hyperbolic geometry-based two-sample test with existing trigonometric methods in circular statistics. Classical procedures rely on Euclidean embeddings of

angular data through trigonometric functions and normal approximation, whereas the proposed approach models the von Mises parameter space directly within a hyperbolic geometric framework. This distinction is particularly relevant in settings involving heterogeneous concentration parameters or combined location-concentration alternatives. The simulation design closely follows and extends the settings considered in [Biswas et al. \(2015, 2016a\)](#), thereby ensuring direct comparability with existing results while highlighting the comparisons of the proposed methodology.

3.1 Equal concentration ($\kappa_1 = \kappa_2$)

Under the null hypothesis, the proposed method exhibits accurate control of the empirical size across a wide range of sample sizes, $n = 20, 50, 100, 200$, and concentration levels $\kappa_1 = \kappa_2 \in \{1, 1.5, 3.0\}$; see Figure 2. The empirical sizes are computed using 2500 permutations within each of 1000 Monte Carlo iterations, with mean directions $\mu_1 = \mu_2 \in [0, 2\pi)$ evaluated on an equally spaced grid of width $\pi/10$. Overall, the proposed test demonstrates a high degree of stability in size across all considered settings and shows improved robustness compared to the existing method of [Biswas et al. \(2016a\)](#).

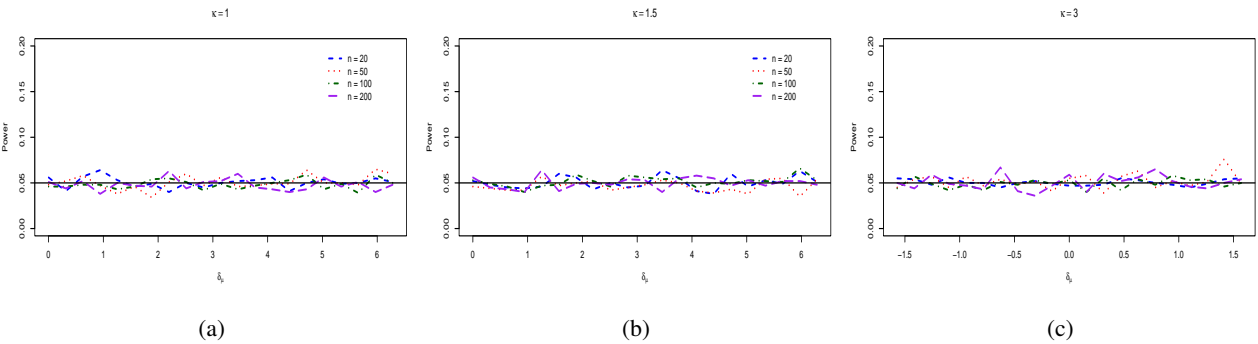


Figure 2: Empirical size at 5% level of the proposed permutation-based test under the null hypothesis for sample sizes $n = 20, 50, 100$, and 200 and equal concentration parameters $\kappa_1 = \kappa_2 \in \{1, 1.5, 3.0\}$, demonstrating accurate size control across settings.

Power curves are subsequently evaluated under the alternative hypothesis $\mu_2 \in [0, 2\pi)$ against the null $\mu_1 = 0$, for the same sample sizes $n = 20, 50, 100, 200$ and concentration parameters $\kappa_1 = \kappa_2 \in \{1, 1.5, 3.0\}$, and are presented in Figure 3[(a),(b),(c)]. For moderate to large sample sizes, the proposed test consistently attains higher empirical power, indicating its favorable asymptotic behavior. For small sample sizes ($n = 20$), the test proposed by [Biswas et al. \(2016a\)](#) exhibits a marginal advantage, while for moderate sample sizes ($n = 50$) the two procedures perform comparably. These differences are further illustrated through the empirical power differences shown in Figure 3[(d),(e),(f)].

3.2 Unequal concentration ($\kappa_1 \neq \kappa_2$)

As the parameter space (see Equation 1.1) and the test statistic (see Equation 2.5) have been defined in the previous section, equal angular separation of the mean from the zero direction still represents non-null situation even when concentration parameters are unequal. As a consequence the empirical size of the above defined permutation test does not match with that of the desired size. Hence we propose to approximate the null distribution with parametric bootstrap and perform the test as required.

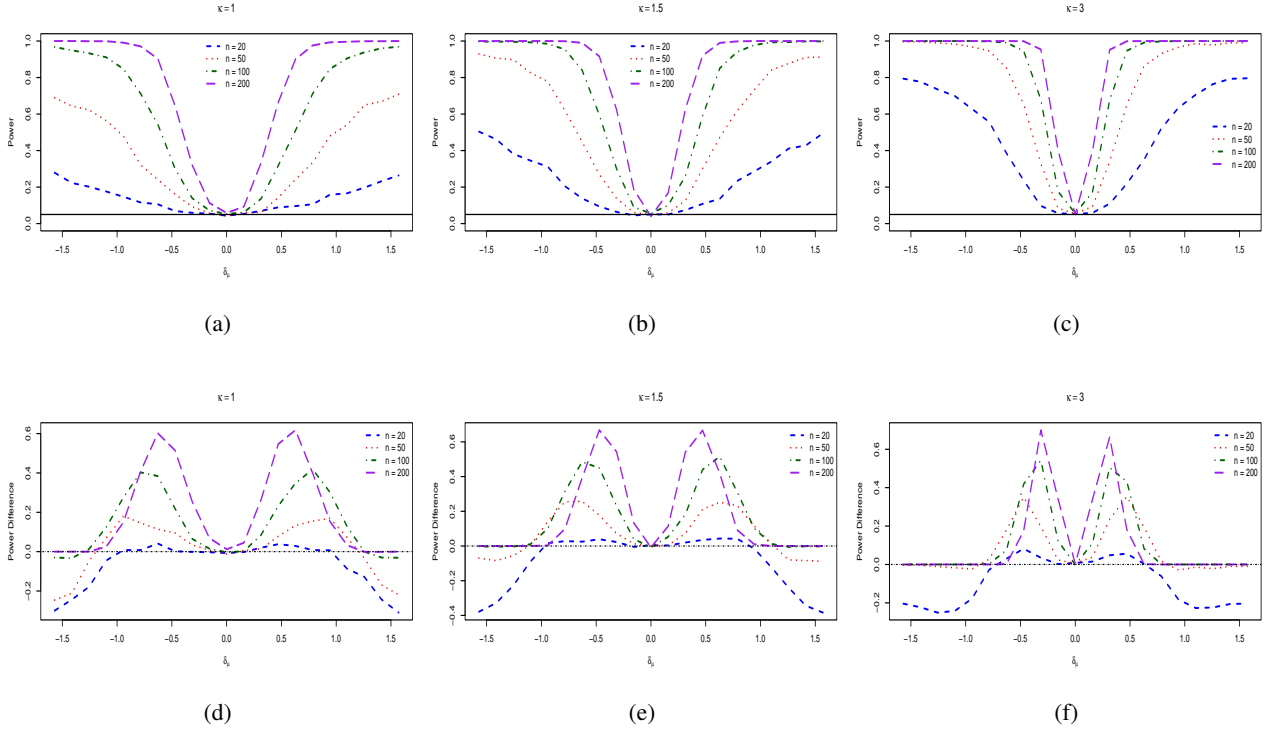


Figure 3: Empirical power curves under the alternative $\mu_2 \in [0, 2\pi)$ with $\mu_1 = 0$ for sample sizes $n = 20, 50, 100$, and 200 and equal concentration parameters $\kappa_1 = \kappa_2 \in \{1, 1.5, 3.0\}$. Panels (a)–(c) show the power curves, while panels (d)–(f) display the corresponding empirical power differences with the Z-test of [Biswas et al. \(2016b\)](#).

For each sample, the parameters (μ_g, κ_g) are estimated by maximum likelihood, yielding $(\hat{\mu}_g, \hat{\kappa}_g)$. The observed test statistic is defined as $T_{\text{obs}} = |d_{R_0}(\hat{\xi}_1) - d_{R_0}(\hat{\xi}_2)|$ from the Equation 2.5.

To approximate the sampling distribution of T_{obs} , a parametric bootstrap procedure is employed. For $b = 1, \dots, B$, independent bootstrap samples are generated according to

$$\theta_{1,i}^{*(b)} \sim \text{vM}(0, \hat{\kappa}_1), \quad \theta_{2,i}^{*(b)} \sim \text{vM}(0, \hat{\kappa}_2),$$

for $i = 1, \dots, n_1$ and $i = 1, \dots, n_2$, respectively. For each bootstrap sample, the von Mises parameters are re-estimated, yielding $(\hat{\mu}_g^{*(b)}, \hat{\kappa}_g^{*(b)})$, and the bootstrap test statistic $T^{*(b)} = |d_{R_0}(\hat{\xi}_1^{*(b)}) - d_{R_0}(\hat{\xi}_2^{*(b)})|$ is computed, where $\hat{\xi}_g^{*(b)} = \xi(\hat{\mu}_g^{*(b)}, \hat{\kappa}_g^{*(b)})$ for $g = 1, 2$.

The two-sided p -value is obtained as

$$p = \frac{1 + \sum_{b=1}^B \mathbb{I}(|T^{*(b)}| \geq |T_{\text{obs}}|)}{B + 1}.$$

The proposed test leverages the intrinsic geometry of the Poincaré disk to encode concentration differences as radial depths, yielding a statistic with a clear geometric interpretation. Owing to its dependence solely on the radial component of the embedding, the test is rotation invariant, which justifies centering the bootstrap samples at zero without loss of generality. By re-estimating the von Mises parameters within each bootstrap replicate, the procedure automatically incorporates estimation uncertainty and avoids reliance on potentially inaccurate asymptotic approximations. The parametric bootstrap further provides a practical solution to the nonlinearity induced by the Poincaré mapping, for

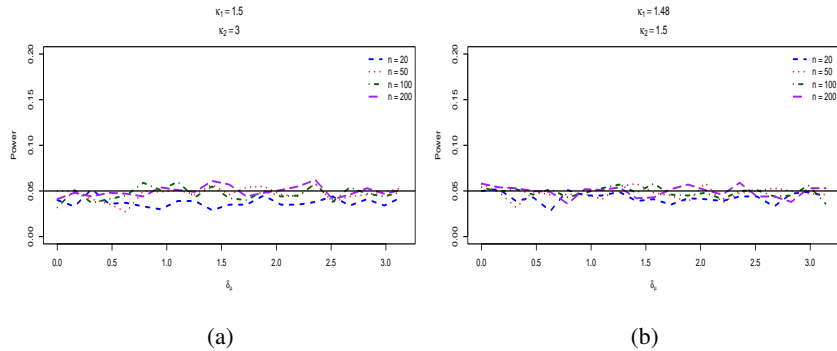


Figure 4: Empirical size under the null hypothesis $\mu_1 = \mu_2 = \mu_2 \in [0, \pi)$ for sample sizes $n = 20, 50, 100$, and 200 , assuming unequal concentration parameters. Panels (a) and (b) correspond to $(\kappa_1, \kappa_2) = (1.5, 3.0)$ and $(1.48, 1.50)$, respectively.

which analytical sampling distributions are intractable. Unlike permutation-based methods, the proposed approach does not rely on exchangeability of the pooled samples, but instead constructs the null distribution through model-based resampling from the fitted von Mises distributions.

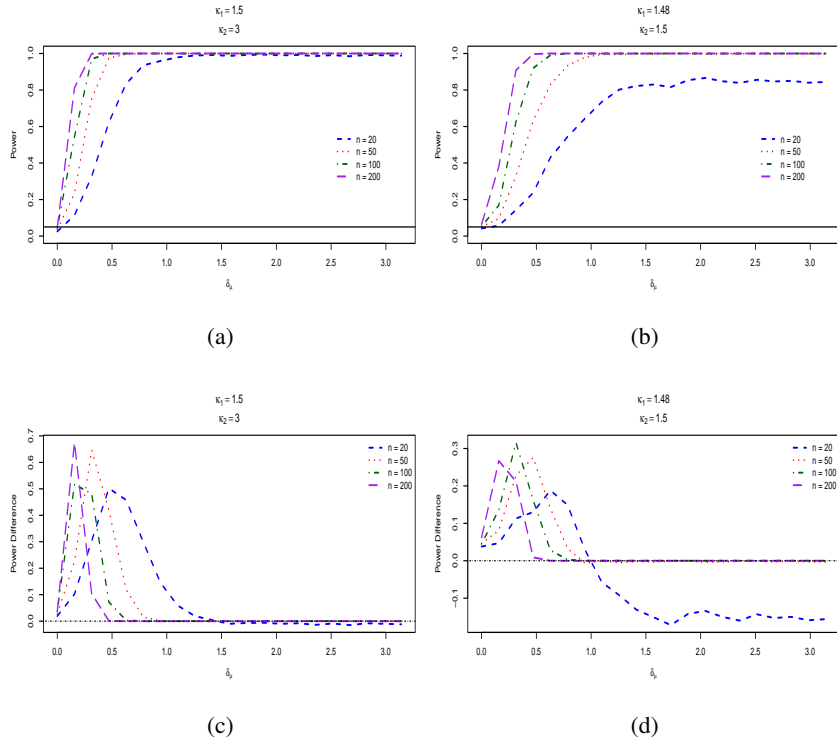


Figure 5: Empirical power curves under the alternative $\mu_2 \in [0, \pi)$ with $\mu_1 = 0$ for sample sizes $n = 20, 50, 100, 200$, assuming unequal concentration parameters. Panels (a) and (b) correspond to $((\kappa_1, \kappa_2) = (1.5, 3.0))$ and $(1.48, 1.50)$, respectively, while panels (c) and (d) show the corresponding empirical power differences with the existing W-test by Biswas et al. (2016a), respectively.

The finite-sample size performance of the proposed test was evaluated through an extensive Monte Carlo simulation study over a broad range of null parameter configurations. For each configuration, 1000 Monte Carlo iterations were conducted, and within each iteration the null distribution of the test statistic was approximated using 2500 parametric bootstrap replicates. The null parameter space included mean directions spanning $\mu \in [0, \pi)$ and concentration parameters covering the range of practical interest encountered in directional data applications. Across all settings considered, the empirical type I error rates were stable and closely matched the nominal significance level, indicating that the bootstrap calibration provides reliable size control in finite samples (see Figure-4). These results demonstrate that the proposed procedure is robust with respect to both angular location and concentration under the null hypothesis, supporting its suitability for routine applied use.

Power curves are evaluated under the alternative hypothesis $\mu_2 \in [0, \pi)$ against the null hypothesis $\mu_1 = 0$, for common sample sizes $n = 20, 50, 100, 200$ and unequal concentration parameters $\kappa_1 = 1.5 \neq \kappa_2 = 3.0$. The resulting power curves are displayed in Figure 5(a). For moderate to large sample sizes, the proposed test consistently achieves higher empirical power, reflecting its favorable asymptotic behavior. These differences are further highlighted by the empirical power differences shown in Figure 5(c). A similar analysis is conducted for the closer concentration parameters $\kappa_1 = 1.48 \neq \kappa_2 = 1.50$, with results presented in Figure 5(b). In this setting, the test proposed by [Biswas et al. \(2016a\)](#) shows a slight advantage for small sample sizes ($n = 20$), whereas for moderate sample sizes ($n = 50$) the two procedures perform comparably, as evidenced by the empirical power differences in Figure 5(d).

4 Data Analysis

Corneal incisions created during cataract surgery can induce changes in corneal curvature. This results in surgically induced astigmatism (SIA). In the present dataset, this effect was observed exclusively in cases undergoing small incision cataract surgery (SICS), irrespective of whether the nucleus was delivered using the VERTICS or SNARE technique. No measurable astigmatic change was detected following Conventional or Torsional Phacoemulsification. Consequently, subsequent data analyses are confined to SICS cases performed using the VERTICS and SNARE techniques.

A prospective, randomized, comparative interventional study was conducted at the Disha Eye Hospital and Research Centre, Barrackpore, West Bengal, India, between 2008 and 2010 (see [Bakshi, 2010](#)). The study included 40 eyes from 40 patients, who were randomly allocated into two equal groups. Twenty patients underwent small incision cataract surgery (SICS) using the SNARE technique, while the remaining twenty underwent SICS using the irrigating VERTICS technique. The dataset analyzed in this study comes with a single preoperative measurement of the astigmatism axis, followed by postoperative measurements at one month and three months. Three observations were missing at the three-month follow-up. These missing axis values were imputed using the circular mean of the available three-month postoperative measurements. Following imputation, the dataset contains complete observations for all 20 VERTICS and 20 SNARE cases. It enables a comprehensive analysis of postoperative astigmatic changes over time across the two surgical techniques. Given the small number of missing values, circular mean imputation was considered appropriate. However, in larger studies with a higher proportion of missing directional data, multiple-imputation approaches that explicitly account for the axial nature of astigmatism measurements would be more suitable. Figures 6(a) and 6(b) present rose diagrams of the astigmatism axis, transformed by quadrupling the angles and reducing them modulo 2π , at the three-month postoperative visit for the SNARE and VERTICS techniques, respectively.

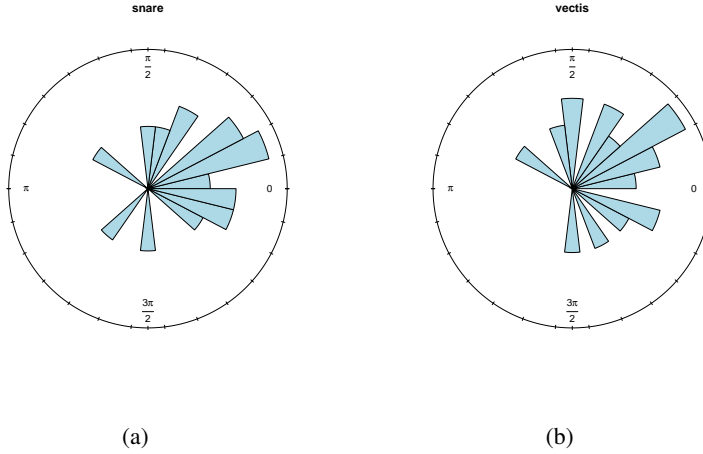


Figure 6: Rose-diagram of SICS data using (a) SNARE technique, and (b) irrigating VERTICS technique.

Separate von Mises distributions were fitted to the astigmatism axis data for the two surgical techniques. For the SNARE technique, the estimated mean direction and concentration parameters were $\hat{\mu}_S = 0.3066$ radians and $\hat{\kappa}_S = 1.560$, respectively. For the irrigating VERTICS technique, the corresponding estimates were $\hat{\mu}_V = 0.5402$ radians and $\hat{\kappa}_V = 1.581$. Figure 3(b) of [Biswas et al. \(2016a\)](#) illustrates the fitted von Mises densities for both techniques under assumptions of common concentration (solid curves) and unequal concentrations (dashed curves); an analogous plot can be generated for the present analysis. For the proposed testing, in neither case was the null hypothesis rejected, with p-values of 0.5891 for the test allowing unequal concentrations and 0.6204 for the test assuming equal concentrations. These results indicate no statistically significant difference between the SNARE and irrigating VERTICS techniques with respect to the axis of surgically induced astigmatism in the available data. More broadly, while the SNARE technique has been reported to yield superior immediate postoperative outcomes for certain clinical measures, long-term results are generally comparable between the two techniques [Bakshi \(2010\)](#). Consistent with this, the SNARE technique appears numerically more favorable in terms of astigmatism axis alignment; however, this apparent advantage does not reach statistical significance.

5 Discussion and Conclusion

We have proposed a new hyperbolic geometric framework for two-sample inference on circular data, motivated by the analysis of angular biomarkers in biomedical studies. By embedding the parameter space of the von-Mises distribution into the Poincaré disk, this work provides, to our knowledge, the first principled application of hyperbolic geometry to statistical inference for circular distributions. The embedding establishes a continuous one-to-one correspondence between distributional parameters and points in Poincaré disk, thereby preserving the intrinsic structure of the model and enabling meaningful distance-based comparisons.

The induced Poincaré distance yields a natural metric for assessing distributional differences and leads to permutation and bootstrap based tests accommodating both equal and unequal concentration parameters respectively. Extensive simulation studies demonstrate that the proposed procedures maintain stable empirical size across a broad range of sample sizes and concentration levels, while achieving superior asymptotic power relative to existing methods. Although

competing tests may perform comparably in very small samples, the proposed approach consistently dominates as sample size increases, underscoring its efficiency and robustness.

The practical value of the methodology is illustrated through an analysis of astigmatism data from cataract surgery patients, following a clinically informed restructuring of the original dataset. The results align with the simulation findings and show that the hyperbolic framework delivers interpretable and clinically relevant conclusions beyond those obtainable with conventional circular tests.

In summary, this study establishes hyperbolic geometry as a coherent and effective foundation for circular data analysis in medical research. The proposed framework is readily extensible to more complex settings, including multi-sample inference and regression models, and offers a promising direction for the analysis of angular data in biostatistics.

References

Bakshi, P. (2010). Evaluation of various surgical techniques in brunescent cataracts. *Unpublished thesis, Disha Eye Hospital, India*, 3.

Banerjee, B. and Biswas, S. (2026). Intrinsic geometry-inspired dependent toroidal distribution: Application to regression model for astigmatism data. *Computational Statistics*, 41(2):37.

Biswas, A., Dutta, S., Laha, A. K., and Bakshi, P. K. (2015). Response-adaptive allocation for circular data. *Journal of Biopharmaceutical Statistics*, 25(4):830–842.

Biswas, A., Dutta, S., Laha, A. K., and Bakshi, P. K. (2016a). Comparison of treatments in a cataract surgery with circular response. *Statistical Methods in Medical Research*, 25(5):2238–2249.

Biswas, A., Dutta, S., Laha, A. K., and Bakshi, P. K. (2016b). Comparison of treatments in a cataract surgery with circular response. *Statistical Methods in Medical Research*, 25(5):2238–2249.

Do Carmo, M. P. and Flaherty Francis, J. (1992). *Riemannian geometry*, volume 2. Springer.

Keener, G. (1995). The nucleus division technique for small incision cataract extraction. *Cataract Surgery: Alternative Small Incision Techniques. 1st ed. New Delhi, India: Jaypee Brothers*, pages 163–191.

Kelman, C. D. (2018). Phaco-emulsification and aspiration: a new technique of cataract removal: a preliminary report. *American journal of ophthalmology*, 191:xxx–xl.

Mardia, K. V. (2000). Directional statistics. *New York: John Wiley and Sons*.

Mardia, K. V. and Jupp, P. E. (2000). *Directional statistics*, volume 2. Wiley Online Library.

Phipson, B. and Smyth, G. K. (2010). Permutation p-values should never be zero: Calculating exact p-values when permutations are randomly drawn. *Statistical Applications in Genetics and Molecular Biology*, 9(1).

Romano, J. P. (1989). Bootstrap and randomization tests of some nonparametric hypotheses. *The Annals of Statistics*, 17(1):141–159.

Srinivasan, A. (2009). Nucleus management with irrigating vectis. *Indian Journal of Ophthalmology*, 57(1):19–21.

6 Appendix

6.1 Proof of Lemma 1 (Uniqueness of Minimizer).

Proof. Consider the function $h_\xi(t) := d_{\mathbb{H}}(\xi, te^{i\mu_0})$ for fixed $\xi \in \mathbb{D}$. The Poincaré disk (\mathbb{D}, d_H) is a strictly convex metric space. In such spaces the set R_{μ_0} forms a geodesic ray from the origin toward the boundary of \mathbb{D} , which is a convex subset of \mathbb{D} . The squared distance function $t \mapsto [h_\xi(t)]^2$ is strictly convex in t (see [Do Carmo and Flaherty Francis, 1992](#)). Therefore, $h_\xi(t)$ is strictly convex on $[0, 1]$. Additionally, $h_\xi(t)$ is continuous on $[0, 1]$ and $\lim_{t \rightarrow 1^-} h_\xi(t) = \infty$ (since the hyperbolic distance diverges as we approach the boundary). A strictly convex, continuous function on a convex domain achieves at most one minimum. Thus, $\mathcal{P}_{\mu_0}(\xi)$ is unique. \square

6.2 Proof of Lemma 2 (Projection along zero direction)

Proof. Following the Equation 1.2 consider the distance between any $\xi \in \mathbb{D}$ and a point $w_0(t) \in R_0 = \{(t, 0) : 0 \leq t < 1\}$

$$d_{\mathbb{D}}(\xi, w_0(t)) = \cosh^{-1} \left(1 + \frac{2(|\xi|^2 + t^2 - 2t\Re(\xi))}{(1 - |\xi|^2)(1 - t^2)} \right).$$

Taking cosh on both sides, we get

$$\cosh(d_{\mathbb{D}}(\xi, w_0(t))) = \left(1 + \frac{2(|\xi|^2 + t^2 - 2t\Re(\xi))}{(1 - |\xi|^2)(1 - t^2)} \right).$$

Differentiating with respect to t and equating to 0, we obtain

$$\sinh(d_{\mathbb{D}}(\xi, w_0(t))) \cdot \frac{d}{dt} d_{\mathbb{D}}(\xi, w_0(t)) = \frac{4(1 - |\xi|^2)[t(1 + |\xi|^2) - \Re(\xi)(1 + t^2)]}{(1 - |\xi|^2)^2(1 - t^2)^2} = 0$$

which leads to

$$\Re(\xi) t^2 - (|\xi|^2 + 1)t + \Re(\xi) = 0.$$

The above quadratic equation has the real root

$$t = \frac{(|\xi|^2 + 1) - \sqrt{(|\xi|^2 + 1)^2 - 4\Re(\xi)^2}}{2\Re(\xi)}$$

with a projection on R_0 as

$$\mathcal{P}_{R_0}(\xi) = \left(\min \left\{ 1, \max \left\{ 0, \frac{1 + |\xi|^2 - \sqrt{(1 + |\xi|^2)^2 - 4\Re(\xi)^2}}{2\Re(\xi)} \right\} \right\}, 0 \right).$$

\square

6.3 Proof of Theorem 1 (Consistency of the Poincaré Distance-Based Permutation Test)

Proof. The proof proceeds by establishing convergence of the test statistic to a non-zero constant under H_1 and exploiting the invariance of the permutation distribution under H_0 .

For each group $g = 1, 2$, the von Mises distribution with $\kappa_g > 0$ is identifiable and belongs to a regular exponential family. Consequently, the maximum likelihood estimators satisfy

$$\hat{\mu}_g \xrightarrow{P} \mu_g, \quad \hat{\kappa}_g \xrightarrow{P} \kappa_g, \quad \text{as } n_g \rightarrow \infty.$$

In particular, since $\bar{R}_g \xrightarrow{P} A_1(\kappa_g)$ by the Law of Large Numbers (where the expectation $\mathbb{E}[e^{i\Theta_g}] = A_1(\kappa_g)e^{i\mu_g}$ for $\Theta_g \sim \text{VM}(\mu_g, \kappa_g)$ is standard in directional statistics; see [Mardia \(2000\)](#), and $A_1(\kappa) = I_1(\kappa)/I_0(\kappa)$ is strictly increasing and continuous on $(0, \infty)$, the estimator $\hat{\kappa}_g = A_1^{-1}(\bar{R}_g)$ is consistent by the continuous mapping theorem. This ensures the consistency of the parameter estimators.

The mapping $\xi : [0, 2\pi) \times [0, \infty) \rightarrow \mathbb{D}$ defined by $\xi(\mu, \kappa) = r(\kappa)e^{i\mu}$ as specified in Equation 1.1 is deterministic and continuous. Hence, by the continuous mapping theorem, $\hat{\xi}_g = \xi(\hat{\mu}_g, \hat{\kappa}_g) \xrightarrow{P} \xi(\mu_g, \kappa_g) = \xi_g$, $g = 1, 2$, satisfying the consistency of the hyperbolic embedding. Uniqueness and continuity of the distance functional is established in Lemma 1. By the uniqueness of the minimizer and continuity of $d_{\mathbb{H}}$, the map $d_{R_0} : \mathbb{D} \rightarrow \mathbb{R}^+$ is continuous on \mathbb{D} . Therefore, $d_{R_0}(\hat{\xi}_g) \xrightarrow{P} d_{R_0}(\xi_g)$, $g = 1, 2$.

Now by Slutsky's theorem, $T = |d_{R_0}(\hat{\xi}_1) - d_{R_0}(\hat{\xi}_2)| \xrightarrow{P} \Delta := |d_{R_0}(\xi_1) - d_{R_0}(\xi_2)|$. Under H_1 , we have $\Delta \neq 0$ by assumption, so for any $\varepsilon > 0$, $\mathbb{P}_{H_1}(T > \varepsilon) \rightarrow 1$ as $\min\{n_1, n_2\} \rightarrow \infty$.

Under H_0 , the joint distribution of the pooled sample $\{\Theta_{1i}\}_{i=1}^{n_1} \cup \{\Theta_{2i}\}_{i=1}^{n_2}$ is invariant under permutations of the group labels. By a standard result in permutation test theory (see [Phipson and Smyth \(2010\)](#), [Romano \(1989\)](#)), the permutation distribution of T and the critical value c_α^{perm} (the $(1 - \alpha)$ -quantile) satisfy:

$$\mathbb{P}_{H_0}(T > c_\alpha^{\text{perm}}) \rightarrow \alpha \quad \text{as } \min\{n_1, n_2\} \rightarrow \infty.$$

Under H_1 , $T \xrightarrow{P} \Delta > 0$. The permutation critical value c_α^{perm} is bounded by the asymptotic quantile under H_0 , which remains $O_P(1)$ and hence strictly less than Δ for large n_1, n_2 . Therefore,

$$\mathbb{P}_{H_1}(|T| > c_\alpha^{\text{perm}}) \rightarrow 1 \quad \text{as } \min\{n_1, n_2\} \rightarrow \infty,$$

establishing consistency of the permutation test. □